ADVANCED FUNCTIONAL MATERIALS
www.afm-journal.de

Sea-Urchin-Inspired 3D Crumpled Graphene Balls Using Simultaneous Etching and Reduction Process for High-Density Capacitive Energy Storage

Jang Yeol Lee, Kwang-Hoon Lee, Young Jin Kim, Jeong Sook Ha, Sang-Soo Lee, and Jeong Gon Son**

A crumpled configuration of graphene is desirable for preventing irreversible stacking between individual nanosheets, which can be a major hurdle toward its widespread application. Herein a sea-urchin-shaped template approach is introduced for fabricating highly crumpled graphene balls in bulk quantities with a simple process. Simultaneous chemical etching and reduction process of graphene oxide (GO)-encapsulated iron oxide particles results in dissolution of the core template with spiky morphology and conversion of the outer GO layers into reduced GO layers with increased hydrophobicity which remain in contact with the spiky surface of the template. After completely etching, the outer graphene layers are fully compressed into the crumpled form along with decrease in total volume by etching. The crumpled balls exhibit significantly larger surface area and good water-dispersion stability than those of stacked reduced GO or other crumple approaches, even though they also show comparable electrical conductivity. Furthermore, they are easily assembled into 3D macroporous networks without any binders through typical processes such as solvent casting or compression molding. The graphene networks with less pore volume still have the crumpled morphology without sacrificing the properties regardless of the assembly processes, producing a promising active electrode material with high gravimetric and volumetric energy density for capacitive energy storage.

1. Introduction

Chemically derived graphene oxide (GO) and its derivatives are promising candidates for a variety of carbon-based functional nanostructures and hybrid architectures because of their unique characteristics that include high theoretical surface area, tunable electrical conductivity, excellent solution processability, and high mass producibility at low cost.[1–4] However, the irreversible stacking due to the strong π–π interactions between graphene nanosheets during drying or reduction processes significantly decreases the solution processability as well as accessible surface area[1–3,5–7] and has been a major obstacle toward the practical application of graphene and GO derivatives.[3–8] A number of strategies have been attempted to prevent the stacking phenomenon, such as controlling the graphene–solvent interaction, exfoliating graphene through lyophilization, and introducing dispersing or spacer additives.[3–5,9–12] Among them, the incorporation of spacer additives such as nanotubes or nanowires between graphene nanosheets has been focused because of the simple process required as well as the adaptability of the process for mass production.[10–12] However, partial restacking is inevitable owing to the dimensional difference between the spacers and nanosheets,[11,12] and segregation or bundling of graphene and spacers from the chemically dissimilar hybridization changes the intrinsic properties of graphene and GO derivatives.[12,13]

Constructing 3D nanostructures of the chemically derived graphene itself could be a simple solution for dealing with the problems described above.[4,14–16] By crumpling the 2D paper-like graphene or GO derivatives,[17–19] the resulting 3D structures can exhibit outstanding aggregation- and compression-resistant properties.[7,19,20] Crumpled GO derivatives have been prepared by several approaches including thermal expansion, cooling construction, substrate regulation, and capillary compression;[7–9,16,21–23] however, many resulting products still show only partially wrinkled and folded 2D sheet structures or nonredispersible agglomerates with nonscalable processes.[16] Recently, Huang and co-workers demonstrated that freestanding crumpled graphene balls can be easily prepared by rapidly drying aerosols of GO suspensions.[7] While this aerosol-assisted crumpled graphene is simply formed through the capillary force of the suspension droplets,[18] the mechanically crumpled structures also require an additional exfoliation

Dr. J. Y. Lee, Dr. K.-H. Lee, Y. J. Kim, Dr. S.-S. Lee, Dr. J. G. Son
Photo-Electronic Hybrids Research Center
Korea Institute of Science and Technology
Seoul 136-791, Republic of Korea
E-mail: s-slee@kist.re.kr; jgson@kist.re.kr
Y. J. Kim, Prof. J. S. Ha, Prof. S.-S. Lee
KU-KIST Graduate School of Converging Science and Technology
Korea University
Seoul 136-701, Republic of Korea

DOI: 10.1002/adfm.201404507

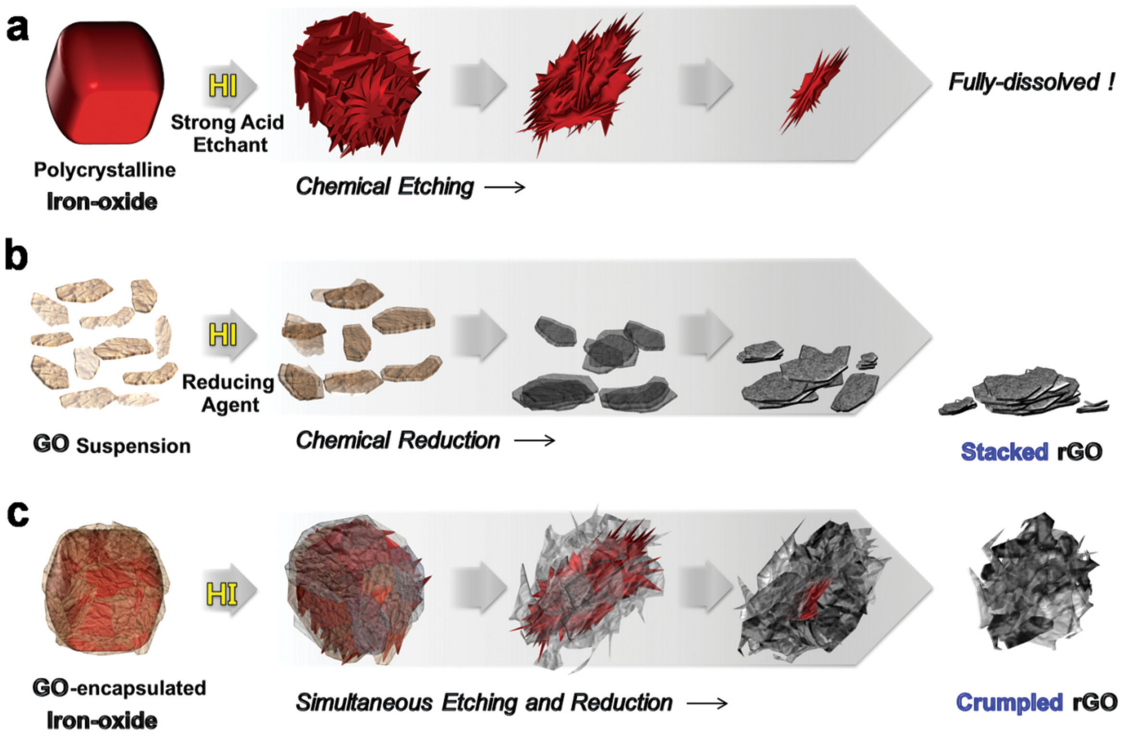

Figure 1. Schematic drawings illustrating the template-guided formation of a 3D crumpled rGO ball. a) A polycrystalline iron-oxide particle is chemically etched by a strong acid etchant HI, resulting in a sea-urchin-shaped dissolving morphology. b) Stacked rGO agglomerates from a GO suspension are chemically reduced, using HI as a reducing agent. c) A highly crumpled rGO ball is formed from a GO@iron-oxide particle with HI treatment through simultaneous chemical etching of the iron oxide core and reduction of the outer GO layers.

process such as thermal shock to enlarge their specific surface area (SSA).[7,12,16]

By assembling 0D, 1D, or 2D materials into well-defined structures such as hollows, foams, and porous scaffolds,[14–16,24–30] the template-guided method has been regarded as a powerful technique for constructing 3D materials. The 3D structures can be easily tailored by adjusting a desired shape of sacrificial hard templates such as metal oxides and polymer colloidal particles.[14,15] Graphene multilayers encapsulating the surface of a hard template can also maintain the original shape of the template before etching.[24–30] However, very thin graphene layers can easily collapse after etching and irreversibly agglomerate with a few wrinkles and folds like a deflated balloon.[24–27] Therefore, the hard-template method for constructing 3D crumpled graphene has rarely been considered.

In this study, we propose an efficient approach to fabricate highly crumpled graphene balls via simultaneous etching and reduction of GO-encapsulated sea-urchin-like particles. Polycrystalline iron-oxide particles are preferentially etched with acids according to their crystal planes,[31–35] and they can form sea-urchin-like spiky microstructures.[31,32] With hydriodic acid (HI) treatment of the GO-encapsulated iron oxide (referred to as GO@iron-oxide hereafter based on the shell@core notation) particles, the GO layers are rapidly converted into reduced GO (rGO) and the hydrophobic rGO layers are tightly and continuously adhered to the sea-urchin-shaped dissolving template. Therefore, the rGO layers can be fully compressed to a heavily crumpled form along with the continuously dissolving spiky template. The template-guided crumpled balls exhibit a large specific surface area, high electrical conductivity, and high water dispersion stability. The crumpled balls can be simply assembled into interconnected 3D macroporous networks by typical solvent casting or compression molding, which also maintains their inherent morphology and properties regardless of the assembly process. These pressed crumpled-graphene networks without any binders also exhibits considerably high gravimetric and volumetric capacitance as an electrochemical electrode for energy-storage devices.

2. Results and Discussion

Figure 1 illustrates the template-guided construction of a hierarchically crumpled rGO structure from GO@iron-oxide particles through a one-step chemical etching–reduction process, which shows spikily etched iron oxide and reduction of outer GO layers. Iron oxide particles have been widely used as selectively etchable templates for various core–shell hybrid structures.[31,34,35] In particular, polycrystalline iron oxides can form a highly spiked exterior with acid dissolution,[31,32] which motivated us to design the 3D crumpled graphene structure in this study. The submicrometer sized and pseudocubic α-Fe_2O_3 particles (JCPDS card no. 33-664, rhombohedral phase) were synthesized in bulk quantities by aging highly condensed

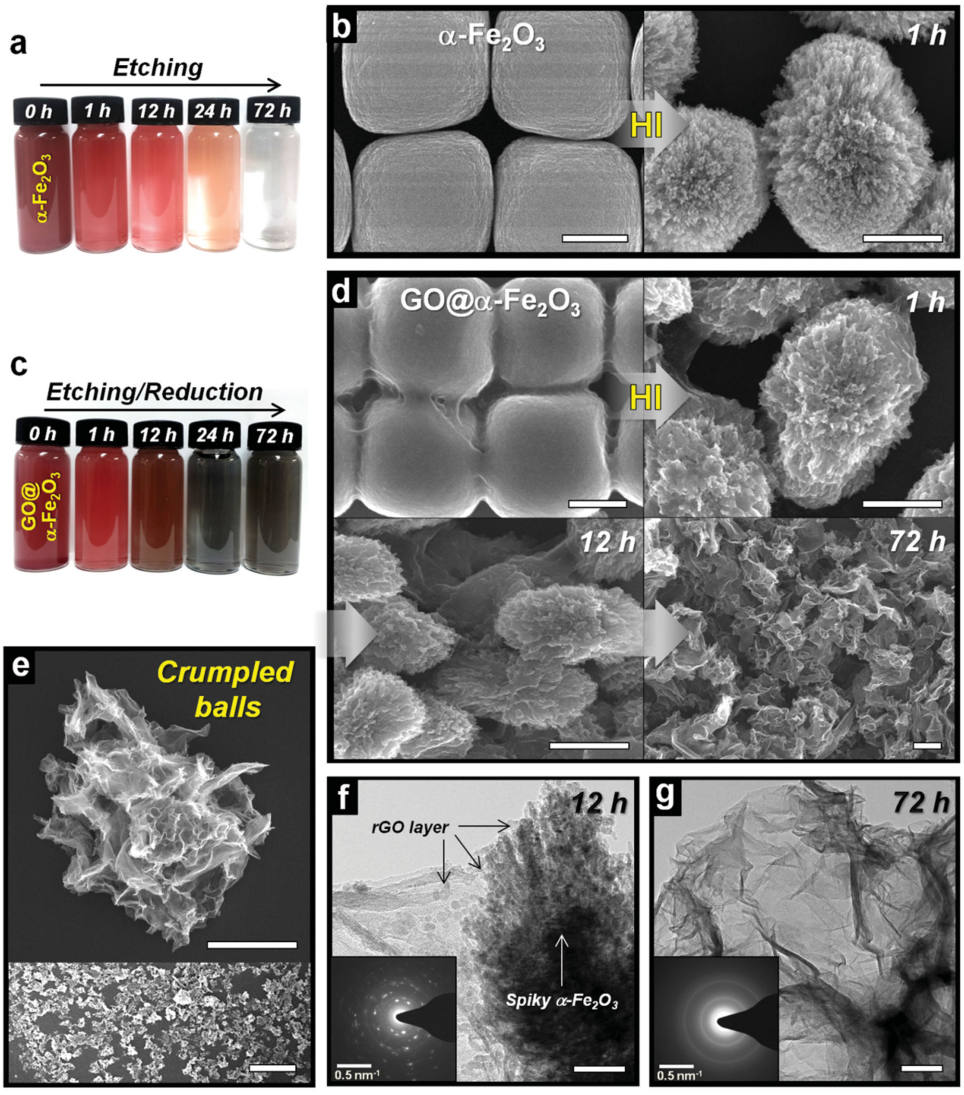

Figure 2. Digital photographs of the HI-treated a) α-Fe_2O_3 and c) GO@α-Fe_2O_3 suspensions with different t_{HI}. SEM images of the b) α-Fe_2O_3 and d) GO@α-Fe_2O_3 particles before and after HI treatment for different t_{HI} (scale bar: 500 nm). e) SEM images of the crumpled balls (scale bar: 2 μm, 100 μm in inset). TEM images and SAED patterns of the f) HI-treated rGO@α-Fe_2O_3 particles and g) crumpled rGO balls (scale bar: 50 nm).

ferric hydroxide gels,[36,37] and they exhibited a polycrystalline structure with a protrusion surface (Figure S1, Supporting Information).[31,37] The α-Fe_2O_3 particles were treated with a polyethyleneimine (PEI) suspension[38] to provide positively charged surface characteristics (ξ = +30 mV) at a neutral pH. The GO nanosheets were obtained using a modified Hummers' method[39] to chemically exfoliate natural graphite and they had a negative charge (ξ = –45 mV) at a neutral pH. Through the electrostatic interaction between the oppositely charged GO and α-Fe_2O_3, a few layered GO nanosheets were assembled on the surface of the α-Fe_2O_3 particles (Figure S1, Supporting Information).

For the template approach, the etching and reduction processes of GO@α-Fe_2O_3 were carried out using a HI reagent that can simultaneously act as an acid etchant of α-Fe_2O_3 and a reducing agent of GO.[40,41] The HI treatments of the α-Fe_2O_3 particles, GO nanosheets, and GO@α-Fe_2O_3 particles were executed at 90 °C for 1–72 h to investigate the effect of the processes on their morphology. The progresses of the etching–reduction with increasing HI treatment time (t_{HI}) were monitored through the macroscopic color change of each suspension[42] and scanning electron microscopy (SEM) images of the resulting particles. The color of the α-Fe_2O_3 suspension changed from reddish-brown to red and then reddish-yellow with increasing t_{HI} (**Figure 2**a) and the color completely faded away after 72 h. The partially dissolved HI-treated α-Fe_2O_3 particles also had a sea-urchin-like spiky appearance, as shown in Figure 2b and illustrated in Figure 1a, which can be attributed to preferential etching of crystal planes with several types of defects such as dislocations, strains, and substitutional impurities in polycrystalline phase.[31] Well-dispersed GO nanosheets in water were chemically reduced by the HI agent, where the iodide as a catalyst could replace oxygen functional groups of GO with organohalides as good leaving groups,[41]

and they were irreversibly stacked because of the strong van der Waals interactions between them (Figure 1b) as previously reported.[1–7,41]

In the case of the GO@α-Fe_2O_3 particles, α-Fe_2O_3 etching and GO reduction occurred simultaneously within the core–shell geometry during the HI treatment. The GO@α-Fe_2O_3 suspension,[42] which was reddish-brown in color owing to the presence of α-Fe_2O_3, gradually turned black from the color of rGO with increasing t_{HI} (Figure 2c). Figure 2d shows representative SEM images of HI-treated GO@α-Fe_2O_3 particles after different t_{HI}. The simultaneous etching–reduction progress promoted the morphological changes of GO@α-Fe_2O_3 particles from pseudocubic to spiky, then fluffy and finally, crumpled structures, as presented in Figure 1c. As shown by the SEM and transmission electron microscopy (TEM) images of the spiky rGO@α-Fe_2O_3 particles (Figure 2d,f, Figure S3, Supporting Information), the outer GO or rGO layers maintained tightly adhered to the spiky surface of the etched α-Fe_2O_3 template, which allowed them to efficiently avoid irreversible stacking. After the etching was completed, the resulting rGO particles exhibited highly porous structures that were composed of many folds and wrinkles with sizes ranging from a few nanometers to several micrometers (Figure 2g and Figure S4, Supporting Information). As a result, the freestanding, several micrometer sized, and highly crumpled rGO balls are successfully fabricated as shown in Figure 2e.

The formation of the individual crumpled-ball structure could be enabled by two characteristics of this approach. First, the GO reduction and α-Fe_2O_3 etching of GO@α-Fe_2O_3 were accomplished at the same time. The HI treatment rapidly converted the negatively charged GO layers to rGO with increased hydrophobicity[3,43] and loosen the electrostatic interaction with PEI attached iron oxide particles. At the same time, reduced GO engages hydrophobic interaction in aqueous solution lead to reduction of hydrated area and volume contraction of rGO shells. Therefore, the rGO balloon structures contracted and adhered tightly and continuously to the dissolving surfaces of α-Fe_2O_3 during the entire process. Second, the polycrystalline α-Fe_2O_3 template exhibited the highly spiky morphology during the etching process. The rGO layers could be guided to the spiky protrusions of the partially dissolved template, which was the origin of the crumpled structure. Finally, the rGO layers were transformed into the highly crumpled balls with their plastic deformations such as folds, ripples, and wrinkles.

To clarify the necessity of the simultaneous etching–reduction process for the crumpling behavior, we additionally executed several control experiments, selective template etching without reduction of the GO layers (Figure S5, Supporting Information) and first-reduction/second-etching experiment (Figure S6, Supporting Information). A sulfuric acid (H_2SO_4) was used for selective etchant of iron oxide[31] without reduction of GO[41] and a hydrazine was used for selective reduction agent of GO without etching iron oxide templates. First, the H_2SO_4-treated α-Fe_2O_3 had dissolving morphology similar to that of the HI-treated α-Fe_2O_3 (Figure S2, Supporting Information). However, unlike the trend shown in the HI treatment, the GO layers were only loosely contacting, not tightly adhering to the partially etched α-Fe_2O_3, and the primarily GO structures that were highly stacked without crumpling were dominantly observed after the H_2SO_4 treatment, as shown in Figure S5 (Supporting Information). Without the hydrophobic interactions, the hydrophilic GO layers could not maintain tight contact with the continuously dissolving template surface, and thereby the structures gradually collapsed and were stacked with each other.[4,6,7,25,43] We also execute the first-reduction/second-etching process using hydrazine for the reduction-only process and sequential H_2SO_4 for the etching, as shown in Figure S6 (Supporting Information). While the HI treated rGO particles individually crumpled and well dispersed in water, the first-reduction/second-etching rGOs were agglomerated and nondispersive in aqueous solution. In SEM images, the first-reduction/second-etching rGOs were also nicely crumpled owing to hydrophobic interaction but massively bundled structures (≈100 μm) rather than individually crumpled structures. Therefore, the hydrophobic interaction should be essential for the crumpled graphene structures but highly crumpled and individually dispersive rGO particles can only be made by simultaneous reduction/etching process using HI treatment.

The structural characteristics of the crumpled graphene balls were investigated using the X-ray diffraction (XRD) patterns obtained at various stages of the α-Fe_2O_3 etching and GO reduction, as shown in **Figure 3**a. The peaks assigned to the rhombohedral α-Fe_2O_3 phase were observed at the early stage of etching process and gradually disappeared with HI treatment. After the treatment, α-Fe_2O_3 peaks were absent while one broad peak was observed at around 22°, indicating the presence of graphitic (002) planes.[40,41] This peak from the crumpled rGO is relatively weak and noticeably broad compared with that of the stacked rGO, which indicates that the rGO structures were almost unstacked.[21–23,40,41] The resulting structures offered a large accessible surface area, which was also confirmed by nitrogen adsorption–desorption analysis (Figure 3b). While rGO from pristine GO and rGO from H_2SO_4 treated GO@α-Fe_2O_3 samples possessed a low SSA of 17 and 32 $m^2\ g^{-1}$, respectively, owing to their nonporous and stacked structures, SSA of the crumpled balls increased significantly to a high value of 496 $m^2\ g^{-1}$, which can be attributed to the removal of α-Fe_2O_3 and the formation of a heavily crumpled structure. The nitrogen adsorption–desorption isotherm of the crumpled rGO showed a typical IV with a little hysteresis loop at a relative pressure of 0.9, revealing the coexistence of macro- and mesopores in the particles, as shown in the SEM and TEM images (Figure 2 and Figure S4, Supporting Information). In addition, SSA of the crumpled rGO was several times higher than the values for aerosol-assisted crumpled GO nanoparticles (82–214 $m^2\ g^{-1}$ without exfoliation),[7,12] which means that when compared to aerosol-assisted capillary compression, the spiky template approach could form a more meticulously crumpled structure.[20]

The chemical reduction of the outer GO layers during the reduction process was evaluated by X-ray photoelectron spectroscopy (XPS) and the results are presented in Figure 3c. High-resolution C1s peaks of GO@α-Fe_2O_3 are assigned to one C—C (284.5 eV) and C—O components including O—C=O (289.3 eV), C=O (288.4 eV), and C—OH/C—O—C (286.7 eV) groups.[1,2,40,41] The peak intensities related to the oxygen-containing groups decreased with increasing t_{HI}, indicating good restoration of delocalized π-conjugation in the graphene

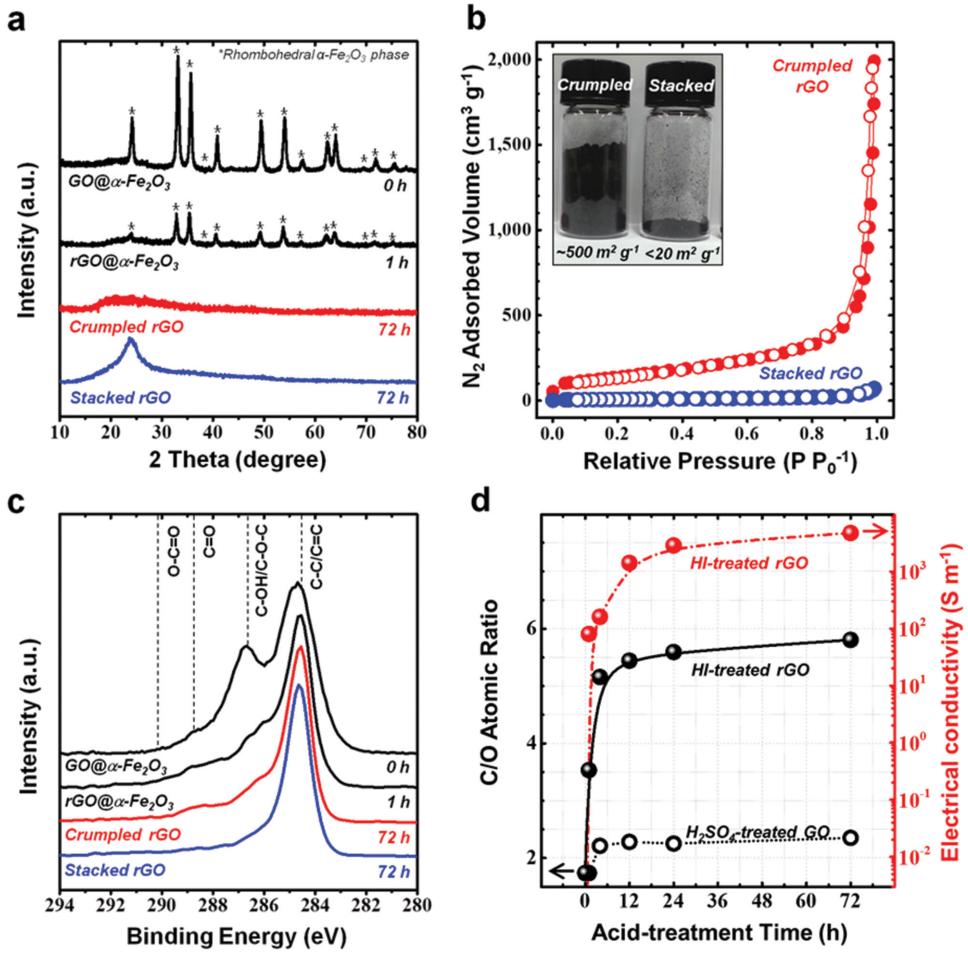

Figure 3. a) XRD patterns of GO@α-Fe_2O_3 (t_{HI} = 0 h), rGO@Fe_2O_3 (t_{HI} = 1 h), crumpled rGO (t_{HI} = 72 h), and stacked rGO prepared without a template (t_{HI} = 72 h). b) Nitrogen adsorption–desorption isotherms of the crumpled rGO and stacked rGO; the inset shows a digital photograph of the two types of rGO powder with the same masses of 100 mg in 10 mL vials. c) XPS C1s spectra of the samples in (a) at various stages of acid treatment. d) C/O atomic ratio and electrical conductivity of the HI- and H_2SO_4-treated particles as functions of acid-treatment time.

sheets.[41] After the complete removal of α-Fe_2O_3, the crumpled rGO exhibited a C1s spectrum similar to that of the stacked rGO. Figure 3d shows the C/O atomic ratio calculated from the XPS results (Figure S7a, Supporting Information) and electrical conductivity as functions of t_{HI}. Before the etching process, the C/O ratio of GO@α-Fe_2O_3 was ≈1.7, slightly lower than pristine GO (≈2.1), because oxygen in iron oxide also affect to oxygen ratio. At the early stage of the reduction process (t_{HI} < 6 h), the oxygen functional groups of the GO layers were considerably removed and the electrical conductivity also significantly increased while the α-Fe_2O_3 template was only partially dissolved. This rapid reduction could have been helpful in inducing the hydrophobic interaction for the template-guided compression of the hydrophobic rGO layers. The crumpled rGO had a the C/O atomic ratio of ≈5.9 and an electrical conductivity of about 4000 S m^{-1} in pelletized form, which are comparable to the values for conventional stacked rGO.[41] On the contrary, the H_2SO_4-treated GO from GO@α-Fe_2O_3 had a C1s spectrum (Figure S7b, Supporting Information) similar to that of pristine GO and its C/O atomic ratio slightly increase with close to the value of pristine GO (≈2.1).

The crumpled rGO particles with this approach are of interest for practical applications because of their suitability for large-scale production, excellent properties, and processability. The GO@iron-oxide precursor, obtained from GO and α-Fe_2O_3, can be synthesized inexpensively in bulk quantities, and the resulting particles are fabricated with high yield by simple and scalable procedures without any complex conditions and post-treatments. (**Figure 4**a) And, the crumpled structure obtained with sea-urchin-inspired template provides a large accessible surface area and high water-dispersion stability. An aqueous suspension with high concentration, shown in Figure 4b, can be prepared by gentle agitation or slight sonication of the crumpled rGO particles in water. Furthermore, the crumpled particles can be assembled easily and rapidly into 3D interconnected macroporous networks by undergoing typical powder processes including solvent casting (Figure 4c), vacuum filtrating (Figure 4d), and compression molding (Figure 4e). These binder-free graphene networks retain the large accessible surface area, high electrical conductivity, and their highly crumpled morphology regardless of the assembly process while the pore volume and densities are drastically changed

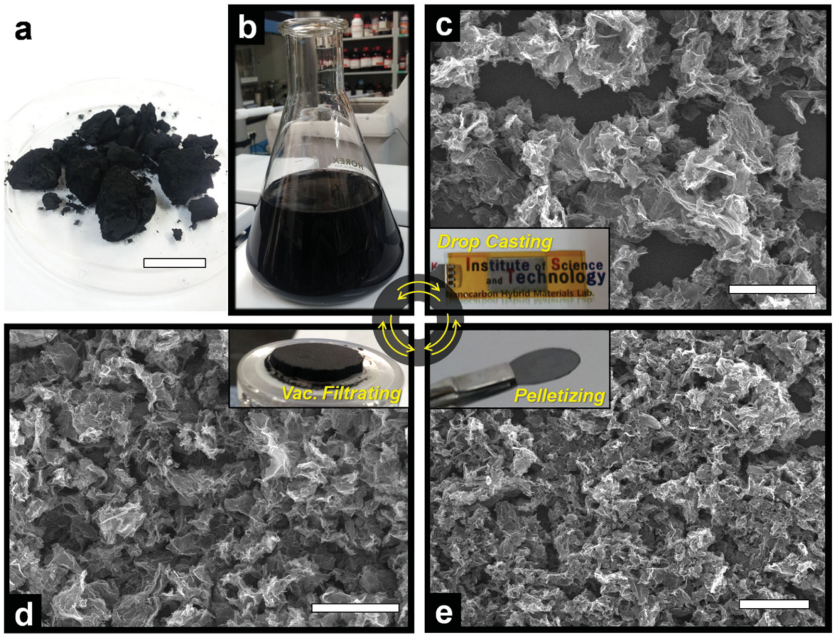

Figure 4. Digital photographs of a) as-produced crumpled rGO particles in bulk quantities (scale bar: 10 mm) and b) aqueous suspension of crumpled rGO particles with a high concentration of 2 mg mL^{-1}. SEM images and (inset) digital photographs of 3D macroporous networks interconnected with the crumpled particles through typical powder processes: c) drop casting, d) vacuum-filtrating, and e) compression molding under a pressure of 50 MPa (scale bar: 10 μm).

(Table S1, Supporting Information). The crumpled particles and networks are readily interchangeable through water dispersion (network disassembly) and solidification (network assembly) within 1 min of processing time (Figure 4b,d), thus allowing nonrestrictive reuse of the material.

These anti-restack properties of crumpled graphene network could be remarkably valuable to the fabrication of graphene-network electrodes for high gravimetric and volumetric capacitive energy storage. When graphene is not encumbered by irreversible stacking, it could be one of the most promising candidates for next-generation electrode materials of energy-storage devices because of its extremely large surface area and high electrical conductivity.[1–3,44] Therefore, we applied differently processed crumpled rGO networks (drop casting, vacuum filtering, and pelletizing) to binder-free electrochemical double-layer capacitor (EDLC) electrodes. The EDLC properties, as shown in **Figure 5**, were evaluated with a typical three-electrode configuration in a 6 M KOH electrolyte. For binder-free formation of the 3D networks, a high-concentration aqueous suspension of the crumpled balls was directly drop casted or vacuum filtered or drop casted then pelletized within nickel foam as a current collector. For control samples, binder-containing crumpled rGO and stacked rGO electrode was prepared with 5 wt% polyvinylidene fluoride (PVDF) as the binder, following previously reported procedures.[45]

Figure 5a shows the cyclic voltammetry (CV) responses of the rGO electrodes with a potential window of 0 to −0.8 V versus an Hg/HgO reference electrode at a sweep rate of 50 mV s^{-1}. The all CV curves showed nearly rectangular shape, indicating typical EDLC behavior of chemically derived graphene.[46] The three binder-free crumpled graphene electrodes showed similarly superior electrochemical capacitance in spite of drastic change of pore volumes, as indicated by maintaining higher capacitances and larger active area, compared to those of the binder-containing crumpled graphene and stacked graphene electrode. The galvanostatic charge–discharge curves of pelletized electrode showed symmetric charge and discharge processes even at high current densities (Figure 5b), indicating the excellent electrochemical features of crumpled graphene as EDLC electrodes and their superior rate capability. As shown in Figure 5c, the values of specific gravimetric capacitance of pelletized, vacuum-filtered, drop-casted crumpled rGO electrodes electrode were ≈396, ≈389, and ≈387 F g^{-1} at a current density of 0.5 A g^{-1}, which is considerably higher than those of the binder-containing crumpled rGO (≈300 F g^{-1}) and stacked rGO (≈72 F g^{-1}) electrodes and other 3D graphene approaches.[47–49] In addition, the specific capacitance of pelletized crumpled-rGO electrode barely changed as the current density were increased from 0.5 to 100 A g^{-1} because the pelletizing process can additionally provide plentiful and stable interfacial contacts and low-electrical-resistance pathways resulting in fast interfacial charge transfer. We also obtained the volumetric capacitance of the electrodes based on their measured density, as can be seen in Figure 5d. While the drop-casted and vacuum-filtered electrodes exhibited fairly low volumetric capacitance because of their sparse structures and low densities, the pelletized crumpled rGO electrode presented particularly high volumetric capacitance (330–321 F cm^{-3} at all current densities, 0.4–83 A cm^{-3}) owing to high packing density, which is much higher value of volumetric capacitance than high density 2D stacked rGO electrode (≈102 F cm^{-3} at 0.7 A cm^{-3} and ≈58 F cm^{-3} at 7.1 A cm^{-3}) and also comparable value with other volumetric capacitor studies.[49–52] Based on these gravimetric and volumetric capacitance, pelletized crumpled-graphene electrode can be an ideal electrode structures for the high energy density supercapacitor devices.

3. Conclusion

In summary, we demonstrated a novel hard-template strategy for the fabrication of highly crumpled graphene balls in bulk quantities via simultaneous chemical etching and reduction of GO@α-Fe_2O_3 particles. The outer GO layers rapidly converted to hydrophobic rGO in the reduction process, thereby maintaining tight adhesion to the α-Fe_2O_3 surface because of the hydrophobic interaction. The hierarchical sea-urchin-like appearance of the α-Fe_2O_3 core during the etching process was also contributed to crumpling of the outer layers. Therefore, the layers were spontaneously transformed into the crumpled balls composed of numerous folds and wrinkles based on their plastic deformations,

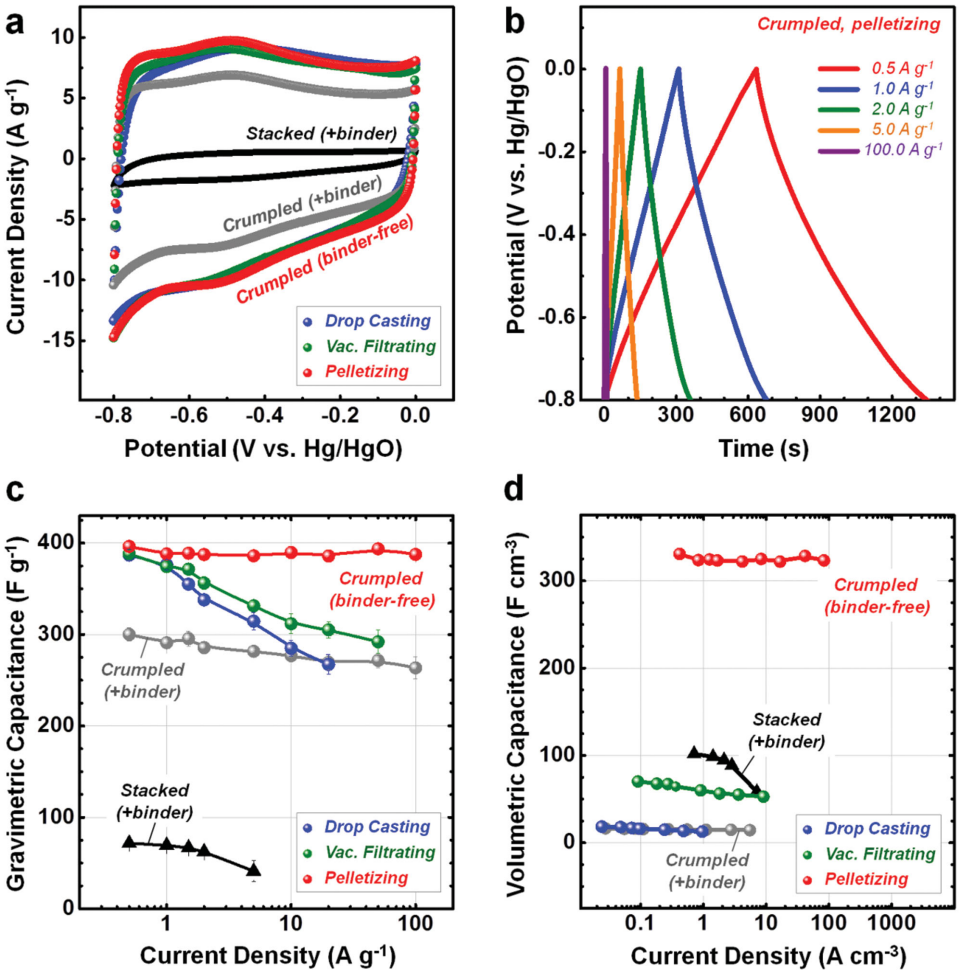

Figure 5. Electrochemical properties with a potential range of 0 and –0.8 V in a 6.0 M KOH electrolyte for the binder-free crumpled rGO electrodes prepared through different processes, the crumpled rGO and the stacked rGO electrodes prepared by using PVDF binder. a) CV curves of the rGO electrodes at a sweep rate of 50 mV s^{-1} and b) charge/discharge curves of the binder-free crumpled rGO electrode in pelletized form at different current densities. c) Gravimetric and d) volumetric capacitances of the rGO electrodes at different current densities.

along with a decrease in total volume by etching. The free-standing and crumpled rGO balls exhibited a much larger accessible surface area and good water-dispersion stability with high electrical conductivity. This template-guided method for synthesizing crumpled balls is useful for large-scale preparation with high yield and it does not require complex process conditions and post-treatments. Using the crumpled balls, the binder-free and high-packing density 3D macroporous networks can be prepared in a simple process and applied to electrochemical electrodes which exhibited superior gravimetric and volumetric capacitance. We expect that our approach will provide a guideline for designing advanced electrode materials of energy-storage devices.

4. Experimental Section

Materials: Reagent-grade ferric chloride hexahydrate ($FeCl_3{\cdot}6H_2O$, 99%), sodium hydroxide (NaOH, >97%), HI (57 wt% in water, distilled, 99.95%), and H_2SO_4 (95%–98%), and hydrazine monohydrate (N_2H_4, 35 wt% in water) supplied from Sigma Aldrich Chemical Co., and all other chemicals were used as received without purification. GO suspension was prepared from natural graphite (Bay Carbon, SP-1 graphite) according to a modified Hummers' methods.[39] Polycrystalline α-Fe_2O_3 particles were prepared by a gel–sol method as described in detail in ref. [36]. Typically, a 100 mL of 5.4 N NaOH aqueous solution was added dropwise with a rate of 0.25 mL s^{-1} into a well-stirred 100 mL aqueous solution of 2.0 N $FeCl_3{\cdot}6H_2O$ in a Pyrex bottle and the mixture was further stirred at 50 °C for another 10 min. The resulting ferric hydroxide gels were then aged at 100 °C for 8 days inside a muffle furnace. The reddish-brown precipitates were washed with deionized water several times to remove any remaining ions. After drying, we obtained more than 10 g of monodisperse pseudocubic α-Fe_2O_3 particles with a diameter of about 1 μm.

Preparation of GO@α-Fe$_2$O$_3$ Particles: GO@α-Fe_2O_3 particles were prepared through the electrostatic interaction between negatively charged GO nanosheets and positively charged α-Fe_2O_3 particles in aqueous solutions, in a similar manner as described in refs.[24–26,28] The positively charged particles were simply prepared by excessively adding a 1 wt% PEI (average $M_w \approx 25$K, branched, Aldrich Chemical Co.) suspension into a 1 wt% aqueous dispersion of the α-Fe_2O_3 particles, and then vigorously stirring overnight at room temperature.[38] The resulting particles were washed by centrifugation and redispersion with deionized water several times to remove unabsorbed PEI. Zeta-potential

measurements (Zetasizer, 3000HSA, Malvern Instruments) confirmed that the PEI-treated particles and GO nanosheets in aqueous suspension at a neutral pH possess the positively and negatively charged surface characteristics, respectively. To assembly a few GO layers onto α-Fe_2O_3 surface, a 0.01 wt% GO suspension was added dropwise with a rate of 1.0 mL s^{-1} into a 1 wt% PEI-treated α-Fe_2O_3 suspension under mild stirring. After several hours, the obtained coagulation was purified by repeated sedimentation and redispersion in deionized water to remove unassembled GO.

Synthesis of Crumpled rGO Particles: The crumpled rGO particles were synthesized from the GO@α-Fe_2O_3 precursor particles by using HI reagent through the one-step etching–reduction process. Typically, a 40 mL of 10 wt% aqueous HI solution was added dropwise under vigorous stirring into a 400 mL aqueous suspension of 10 g GO@α-Fe_2O_3 particles. The resulting mixture empirically had the acidity of about pH 1–2, which is proper for the simultaneous etching–reduction based on the experimental conditions of each α-Fe_2O_3 etching[31–33] and GO reduction[40,41] in the previous reports. The HI treatment was carried out at 90 °C for t_{HI} ranging from 1 to 72 h. The H_2SO_4 treatment for selective etching of α-Fe_2O_3 template without reduction of GO layers was also carried out with the same conditions. For the reduction-only process of GO layers without etching of α-Fe_2O_3 template, GO@α-Fe_2O_3 particles was treated with N_2H_4 at 80 °C for 24 h according to the Wallace method.[5] The stacked rGO as a counterpart of the crumpled rGO was prepared from the pristine GO suspension without the template and with the same procedure of the HI treatment. After HI or H_2SO_4 treatments, the resulting products were isolated by vacuum filtrating and then thoroughly washing with deionized water to remove any remaining acids and ions.

Characterizations: The morphology of the products was investigated through a field-emission SEM (JSM-6701F, JEOL) and a high-resolution TEM (Tecnai F20 G2, FEI) equipped with selected-area electron diffraction (SAED). The crystalline structure and composition were characterized by a powder XRD (D8 ADVANCE, Bruker) with a monochromatized Cu-Kα radiation. The element composition of the GO and rGO layers was analyzed by an XPS (PHI-5000 Versa-Probe, ULVAC-PHI) using a focused monochromatized Al-Kα radiation (1486.6 eV). The degree of reduction of the GO and rGO layers was evaluated by the C/O atomic ratio calculated from the XPS results. The nitrogen adsorption–desorption isotherms were measured at 77 K using a high precision gas/vapor absorption apparatus (Belsorp-Max, BEL Japan Inc.) and the SSA was calculated using a Brunauer–Emmett–Teller method. The electrical conductivity was measured using a four-point probe measurement system (CRESBOX, Napson) and the average values out of at least ten measurements were taken.

Electrochemical Measurements: The electrochemical performance of the rGO electrodes was evaluated by CV and galvanostatic charge/discharge measurements using a potentiostat/galvanostat instrument (PGSTAT-128N, Metrohm Autolab). The working electrodes of the crumpled rGO were fabricated with the various processes, drop casting, vacuum filtrating, and pelletizing. To prepare the binder-free slurry, a 10 wt% crumpled rGO suspension without other additives was vigorously stirred for several hours at 90 °C. The drop-casted electrodes were prepared by repeatedly dropping the crumpled rGO slurry onto nickel foam as a current collector (1 cm^2 in geometric surface area) until the loading of rGO reached 1–2 mg cm^{-2}. The vacuum-filtrated electrodes were prepared by flowing the slurry into nickel foam onto a polymeric filter membrane with vacuuming, and after drying in air, carefully transferring the sediments into the nickel foam with removing the filter membrane. The pelletized electrodes were prepared by compressing the drop casted electrodes under a pressure of 50 MPa. The binder-containing electrodes of the stacked or crumpled rGO were prepared by mixing 95 wt% active materials and 5 wt% polyvinylidene fluoride as a binder with *N*-methylpyrrolidone as a solvent and then spreading the as-prepared slurry onto nickel foam, following the procedure presented in the literature.[45] In a three-electrode configuration using a platinum coil as counter electrode and an Hg/HgO as reference electrode, the electrochemical measurements were performed with a potential window of 0 to −0.8 V at different sweep rates and/or current densities in a 6 M KOH aqueous electrolyte. The gravimetric specific capacitances (C_g) were calculated from the discharging curves at the various gravimetric current densities in the range from 0.5 to 100 A g^{-1} according to the following equation:

$$C_g = \frac{(Im^{-1})\Delta t}{\Delta V} \quad (1)$$

where I, m, Δt, and ΔV are the applied current, the loading mass of rGO materials, the discharging time after IR drop, and the potential window, respectively. The volumetric current densities ($I\nu^{-1}$, where ν is the volume of the rGO) were calculated by using the applied gravimetric current densities (Im^{-1}) during C_g measurements and the obtained densities (d) of the rGO electrode materials, and thereby the volumetric capacitances (C_v) were calculated based on the following equation:

$$C_v = dC_g \quad (2)$$

Supporting Information

Supporting Information is available from the Wiley Online Library or from the author.

Acknowledgements

The authors gratefully acknowledge financial support from the Global Frontier Research Program (2011-0032156) funded by the Korean Government (MEST) and Korea Institute of Science and Technology (KIST) internal project. The authors also would like to acknowledge the financial support from the R&D Convergence Program of NST (National Research Council of Science & Technology) of Republic of Korea.

Received: December 19, 2014
Revised: April 8, 2015
Published online: May 7, 2015

[1] S. Park, R. S. Ruoff, *Nat. Nanotechnol.* **2009**, *4*, 217.
[2] W. Gao, L. B. Alemany, L. Ci, P. M. Ajayan, *Nat. Chem.* **2009**, *1*, 403.
[3] D. R. Dreyer, S. Park, C. W. Bielawski, R. S. Ruoff, *Chem. Soc. Rev.* **2010**, *39*, 228.
[4] R. L. Whitby, *ACS Nano* **2014**, *8*, 9733.
[5] D. Li, M. B. Muller, S. Gilje, R. B. Kaner, G. G. Wallace, *Nat. Nanotechnol.* **2008**, *3*, 101.
[6] Y. J. Dappe, M. A. Basanta, F. Flores, J. Ortega, *Phys. Rev. B* **2006**, *74*, 205434.
[7] J. Y. Luo, H. D. Jang, T. Sun, L. Xiao, Z. He, A. P. Katsoulidis, M. G. Kanatzidis, J. M. Gibson, J. Huang, *ACS Nano* **2011**, *5*, 8943.
[8] J. Luo, H. D. Jang, J. Huang, *ACS Nano* **2013**, *7*, 1464.
[9] F. J. Tölle, M. Fabritius, R. Mülhaupt, *Adv. Funct. Mater.* **2012**, *22*, 1136.
[10] Y. Zhu, L. Li, C. Zhang, G. Casillas, Z. Sun, Z. Yan, G. Ruan, Z. Peng, A.-R. O. Raji, C. Kittrell, R. H. Hauge, J. M. Tour, *Nat. Commun.* **2012**, *3*, 1225.
[11] Y. Wang, Y. Wu, Y. Huang, F. Zhang, X. Yang, Y. Ma, Y. Chen, *J. Phys. Chem. C* **2011**, *115*, 23192.
[12] F. Guo, M. Creighton, Y. Chen, R. Hurt, I. Külaots, *Carbon* **2014**, *66*, 476.
[13] M. Q. Zhao, Q. Zhang, J. Q. Huang, G. L. Tian, J. Q. Nie, H. J. Peng, F. Wei, *Nat. Commun.* **2014**, *5*, 3410.
[14] Y. Xu, G. Shi, *J. Mater. Chem.* **2011**, *21*, 3311.

[15] J. Hong, J. Y. Han, H. Yoon, P. Joo, T. Lee, E. Seo, K. Char, B.-S. Kim, *Nanoscale* **2011**, *3*, 4515.
[16] L. Jiang, Z. Fan, *Nanoscale* **2014**, *6*, 1922.
[17] T. Tallinen, J. A. Astrom, J. Timonen, *Nat. Mater.* **2009**, *8*, 25.
[18] X. Ma, M. R. Zachariah, C. D. Zangmeister, *Nano Lett.* **2011**, *12*, 486.
[19] C. Chang, Z. Song, J. Lin, Z. Xu, *RSC Adv.* **2013**, *3*, 2720.
[20] S. W. Cranford, M. J. Buehler, *Phys. Rev. B* **2011**, *84*, 205451.
[21] M. J. McAllister, J. L. Li, D. H. Adamson, H. C. Schniepp, A. A. Abdala, J. Liu, M. Herrera-Alonso, D. L. Milius, R. Car, R. K. Prud'homme, I. A. Aksay, *Chem. Mater.* **2007**, *19*, 4396.
[22] J. Yan, Y. Xiao, G. Ning, T. Wei, Z. Fan, *RSC Adv.* **2013**, *3*, 2566.
[23] J. H. Lee, N. Park, B. G. Kim, D. S. Jung, K. Im, J. Hur, J. W. Choi, *ACS Nano* **2013**, *7*, 9366.
[24] J. L. Vickery, A. J. Patil, S. Mann, *Adv. Mater.* **2009**, *21*, 2180.
[25] J. Hong, K. Char, B. S. Kim, *J. Phys. Chem. Lett.* **2010**, *1*, 3442.
[26] T. H. Han, W. J. Lee, D. H. Lee, J. E. Kim, E. Y. Choi, S. O. Kim, *Adv. Mater.* **2010**, *22*, 2060.
[27] S. M. Yoon, W. M. Choi, H. Baik, H. J. Shin, I. Song, M. S. Kwon, J. J. Bae, H. Kim, Y. H. Lee, J.-Y. Choi, *ACS Nano* **2012**, *6*, 6803.
[28] S. A. Ju, K. Kim, J. H. Kim, S.-S. Lee, *ACS Appl. Mater. Interfaces* **2011**, *3*, 2904.
[29] B. G. Choi, M. Yang, W. H. Hong, J. W. Choi, Y. S. Huh, *ACS Nano* **2012**, *6*, 4020.
[30] Y. Li, Z. Li, P. K. Shen, *Adv. Mater.* **2013**, *25*, 2474.
[31] R. M. Cornell, U. Schwertmann, *The Iron Oxides: Srtucture, Properties, Reactions, Occurrences and Uses*, 2nd ed., John Wiley & Sons, Weinheim, Germany **2006**.
[32] R. M. Cornell, R. Giovanoli, *Clay Miner.* **1993**, *28*, 223.
[33] H. Majima, Y. Awakura, T. Mishima, *Metall. Trans. B* **1985**, *16*, 23.
[34] Y. Wang, X. Su, S. Lu, *J. Mater. Chem.* **2012**, *22*, 1969.
[35] L. Rossi, S. Sacanna, W. T. Irvine, P. M. Chaikin, D. J. Pine, A. P. Philipse, *Soft Matter* **2011**, *7*, 4139.
[36] T. Sugimoto, K. Sakata, *J. Colloid Interface Sci.* **1992**, *152*, 587.
[37] T. Sugimoto, K. Sakata, A. Muramatsu, *J. Colloid Interface Sci.* **1993**, *159*, 372.
[38] S. Chibowski, J. Patkowski, E. Grządka, *J. Colloid Interface Sci.* **2009**, *329*, 1.
[39] W. S. Hummers Jr., R. E. Offeman, *J. Am. Chem. Soc.* **1958**, *80*, 1339.
[40] K. Moon, J. Lee, R. S. Ruoff, H. Lee, *Nat. Commun.* **2010**, *1*, 73.
[41] a) S. Pei, H. M. Cheng, *Carbon* **2012**, *50*, 3210; b) S. Stankovich, D. A. Dikin, R. D. Piner, K. A. Kohlhaas, A. Kleinhammes, Y. Jia, Y. Wu, S. T. Nguyen, R. S. Ruoff, *Carbon* **2007**, *45*, 1558.
[42] The starting concentration of the aqueous suspensions is 0.25 mg mL^{-1} and the resulting with same volume is taken after washed.
[43] S. Y. Jeong, S. H. Kim, J. T. Han, H. J. Jeong, S. Y. Jeong, G.-W. Lee, *Adv. Funct. Mater.* **2012**, *22*, 3307.
[44] N. Mahmood, C. Zhang, H. Yin, Y. Hou, *J. Mater. Chem. A* **2014**, *2*, 15.
[45] E. Frackowiak, F. Beguin, *Carbon* **2001**, *39*, 937.
[46] J. Hu, Z. Kang, F. Li, X. Huang, *Carbon* **2014**, *67*, 221.
[47] Y. Huang, J. Liang, Y. Chen, *Small* **2012**, *8*, 1805.
[48] L. Dong, Z. Chen, D. Yang, H. Lu, *RSC Adv.* **2013**, *3*, 21183.
[49] T. Y. Kim, G. Jung, S. Yoo, K. S. Suh, R. S. Ruoff, *ACS Nano* **2013**, *7*, 6899.
[50] C. Zhang, W. Lv, Y. Tao, Q.-H. Yang, *Energy Environ. Sci.* **2015**, DOI: 101039/C5EE00389J.
[51] D. Yu, K. Goh, H. Wang, L. Wei, W. Jiang, Q. Zhang, L. Dai, Y. Chen, *Nat. Nanotechnol.* **2014**, *9*, 555.
[52] N. Jung, S. Kwon, D. Lee, D.-M. Yoon, Y. M. Park, A. Benayad, J.-Y. Choi, J. S. Park, *Adv. Mater.* **2013**, *25*, 6854.